Rough viscoelastic sliding contact: Theory and experiments

G. Carbone and C. Putignano
Department of Mechanics, Mathematics and Mangagement, TriboLAB, Politecnico di Bari, Viale Japigia 182, 70126 Bari, Italy
(Received 14 October 2013; revised manuscript received 10 January 2014; published 25 March 2014)

In this paper, we show how the numerical theory introduced by the authors [Carbone and Putignano, J. Mech. Phys. Solids **61**, 1822 (2013)] can be effectively employed to study the contact between viscoelastic rough solids. The huge numerical complexity is successfully faced up by employing the adaptive nonuniform mesh developed by the authors in Putignano *et al*. [J. Mech. Phys. Solids **60**, 973 (2012)]. Results mark the importance of accounting for viscoelastic effects to correctly simulate the sliding rough contact. In detail, attention is, first, paid to evaluate the viscoelastic dissipation, i.e., the viscoelastic friction. Fixed the sliding speed and the normal load, friction is completely determined. Furthermore, since the methodology employed in the work allows to study contact between real materials, a comparison between experimental outcomes and numerical prediction in terms of viscoelastic friction is shown. The good agreement seems to validate—at least partially—the presented methodology. Finally, it is shown that viscoelasticity entails not only the dissipative effects previously outlined, but is also strictly related to the anisotropy of the contact solution. Indeed, a marked anisotropy is present in the contact region, which results stretched in the direction perpendicular to the sliding speed. In the paper, the anisotropy of the deformed surface and of the contact area is investigated and quantified.

DOI: 10.1103/PhysRevE.89.032408 PACS number(s): 81.40.Pq, 46.35.+z, 46.55.+d, 62.20.Qp

I. INTRODUCTION

In a countless number of rubber engineering components, including, *inter alia,* tires, belts, and seals, the viscoelastic mechanical response and the consequent dissipation have to be accurately accounted for. Indeed, the smart design of such elements is a key point in current applied mechanics research: a more efficient design of automotive tires or an improved sealing action for mechanical seals could have a prominent impact in everyday life by providing significant energy savings and improved wear resistance. However, these optimization efforts strictly require an accurate comprehension of the viscoelastic properties of contact problems. As a matter of fact, many scientific contributions have been dedicated to develop theories [1–5] and numerical methodologies [6–15] to investigate rolling, sliding, and lubricated contacts of viscoelastic materials. The huge number of different approaches marks the difficulty of the problem, whose solution is characterized by strongly dissipative effects [13]. A further element boosting this complexity is the roughness between the contacting surfaces. Indeed, the sliding or rolling contact between rough surfaces involves a very large number of length and time scales (covering more than 6 orders of magnitude), which provoke a huge increase of computational complexity and make conventional numerical techniques, including finite element solvers, unfeasible for these types of investigations. On the other side, in the past decade, Persson [2,4,5] has proposed an innovative analytic approach to account for the role played by the roughness and to calculate, among the other quantities, the contact area and the viscoelastic dissipation. In comparison with other rough contact theories and, in particular, with multiasperity models [16–19], one of the main breakthroughs entailed in Persson's model is related to the ability of accounting for the interactions between the different asperities. In detail, Persson's theory shows that the contact pressure probability distribution is governed by a diffusive process as the magnification at which we observe the interface is increased. By means of this result, it is possible to take into account the interaction between the contact spots and to obtain the exact solution in full-contact conditions. In the case of partial contact, the theory is approximate but still provides qualitatively good results. For a more detailed discussion, the reader is also referred to Refs. [20–27].

In this paper, our aim is to show a numerical methodology that could accurately describe the viscoelastic contact of rough surfaces, thus being a powerful tool to validate the analytical models and to study possible practical problems. In detail, by relying on the theory presented by the authors in Ref. [13] and experimentally validated in Ref. [15], we employ a boundary element methodology to study the contact of a rough surface sliding over a viscoelastic half space. Indeed, the computation complexity of the contact domain is conducted by formulating the problem in such a way that only contact spots need to be discretized [20,21] and by employing the adaptive nonuniform mesh developed by the authors in Refs. [24,25]. This scheme allows us to strongly decrease the number of elements needed to solve the problem, thus significantly reducing the computation time. By means of this approach, we are able to elucidate the main aspects marking the viscoelastic sliding motion. Indeed, we start our analysis by calculating the viscoelastic friction due to the sliding of a rigid rough punch over a viscoelastic layer; hence, we compare numerical results with experimental outcomes obtained by studying the sliding of a rubber block over a sandblasted steel plate. Afterwards, we pay attention to the second peculiar aspect of viscoelastic contact mechanics, that is, the contact area anisotropy which occurs during sliding because of viscoelastic effects. Indeed, the contact domain not only reduces due to the material stiffening but also shows the marked anisotropy quantified in the paper.

II. FORMULATION

As shown in detail in Ref. [13], by recalling the translational invariance and the elastic-viscoelastic correspondence

principle [28], we may formulate the general linear-viscoelastic contact problem between a rigid indenter and a viscoelastic slab as follows:

$$u(\mathbf{x},t) = \int_{-\infty}^{t} d\tau \int d^2x' \mathcal{J}(t-\tau)\mathcal{G}(\mathbf{x}-\mathbf{x}')\dot{\sigma}(\mathbf{x}',\tau), \quad (1)$$

where $\mathbf{x}$ is the in-plane position vector, t is the time, $u(\mathbf{x},t)$ is the normal surface displacement of the viscoelastic solid, $\sigma(\mathbf{x},t)$ is the normal interfacial stress, and $\mathcal{G}(\mathbf{x})$ and $\mathcal{J}(t)$ are respectively the Green's function and the creep function. The latter quantity satisfies causality, i.e., $\mathcal{J}(t<0)=0$, and, for a generic viscoelastic material [28], can be written as follows:

$$\mathcal{J}(t) = \mathcal{H}(t)\left[\frac{1}{E_0} - \int_0^{+\infty} d\tau \mathcal{C}(\tau)\exp(-t/\tau)\right], \quad (2)$$

where $\mathcal{H}(t)$ is the Heaviside step function, the real quantity E_0 is the rubber elastic modulus of the material at zero frequency, $\mathcal{C}(\tau)$ is a strictly positive function usually defined as the creep (or retardation) spectrum [28,29], and τ is the relaxation time, continuously distributed on the real axis.

Now, assuming that sliding occurs at constant velocity and neglecting nonuniform temperature effects, one can show that Eq. (1), with the substitution $\mathbf{x} \to \mathbf{x} + \mathbf{v}t$, can be rewritten in the following form:

$$u(\mathbf{x}) = \int d^2x' G(\mathbf{x}-\mathbf{x}',\mathbf{v})\sigma(\mathbf{x}'). \quad (3)$$

The authors have shown in Refs. [13,14] that the kernel $G(\mathbf{x},\mathbf{v})$, which depends parametrically on the sliding speed $\mathbf{v}$, has the following form:

$$G(\mathbf{x},\mathbf{v}) = -\frac{1-\nu^2}{\pi}\left\{\frac{1}{E_\infty}\frac{1}{|\mathbf{x}|}\Theta\left(\frac{|\mathbf{x}|}{h}\right) + \int_0^{+\infty} d\tau C(\tau) \times \int_{0^+}^{+\infty} dz \frac{1}{|\mathbf{x}+\mathbf{v}\tau z|}\Theta\left(\frac{|\mathbf{x}+\mathbf{v}\tau z|}{h}\right)\exp(-z)\right\}, \quad (4)$$

where $\Theta(|\mathbf{x}|/h)$ is a corrective parameter introduced to account for the viscoelastic slab thickness h,

$$\Theta(r/h) = \int_0^{+\infty} dw S(wh/r) J_0(w), \quad (5)$$

with $S(wh/r)$ a correction term which accounts for different constraint or boundary conditions (see Refs. [13,14] for more details) and $J_0(w)$ the zeroth-order Bessel function. We stress that, as should be expected, $\Theta(r/h)$ approaches the unit value at relatively low values of r/h. For further details regarding the mathematical procedure to obtain $G(\mathbf{x},\mathbf{v})$, the reader is referred to Ref. [13]. Finally, we observe that, in order to be closer to the experimental setup employed in the following section to validate the methodology, the formulation proposed for the Green's function is nonperiodic: indeed, the sliding contact of a rough finite pad will be studied. However, if it should be required, periodic conditions could be applied by following the approach suggested by the authors in Ref. [24] for elastic materials, in order to obtain a periodic Green's function.

Interestingly, once the Green's function $G(\mathbf{x},\mathbf{v})$ is explicitly given, the viscoelastic problem can be solved by following the same approach already employed by the authors for elastic contact mechanics [24,25]. This strategy consists in discretizing the contact domain in N square cells and then employing the usual solution scheme for boundary element methodologies. In detail, assuming that in each square cell the normal stress σ is constant and equal to $\sigma_k = \sigma(\mathbf{x}_k)$, where $\mathbf{x}_k$ is the position vector of the center of the square cell D_k, the normal displacement $u_i = u(\mathbf{x}_i)$ at the center of the i-th square cell can be expressed as

$$u_i = -\frac{1-\nu^2}{\pi}\sum_{k=1}^{N}\sigma_k\left\{\Theta\left(\frac{|\mathbf{x}_i-\mathbf{x}_k'|}{h}\right)\frac{1}{E_\infty}\int_{D_k} d^2x' \frac{1}{|\mathbf{x}_i-\mathbf{x}'|} + \int_0^{+\infty} d\tau C(\tau)\int_{0^+}^{+\infty} dz \exp(-z)\Theta\left(\frac{|\mathbf{x}_i+\mathbf{v}\tau z-\mathbf{x}_k'|}{h}\right) \times \int_{D_k} d^2x' \frac{1}{|\mathbf{x}_i+\mathbf{v}\tau z-\mathbf{x}'|}\right\}, \quad (6)$$

where the terms $\int_{D_k} d^2x' |\mathbf{x}_i-\mathbf{x}'|^{-1}$ and $\int_{D_k} d^2x' |\mathbf{x}_i+\mathbf{v}\tau z-\mathbf{x}'|^{-1}$ can be easily calculated by exploiting Love's solution for elastic materials [30], as shown in Ref. [24]. In such a way, the problem is reduced to a system of linear equations of the following type:

$$u_i = L_{ik}(\mathbf{v})\sigma_k, \quad (7)$$

where the response matrix $L_{ik}(\mathbf{v})$ parametrically depends on the velocity $\mathbf{v}$. Equation (7) can be easily solved, together with the determination of the real contact area, by employing the iterative scheme based on a nonuniform adaptive mesh already presented by the authors for the case of elastic materials [24,25]. Such a discretization technique entails strong computational savings and allows us to handle surfaces with a roughness spectrum covering several orders of magnitude of spatial frequencies [24]. It is noteworthy to observe that, in the proposed formulation, we are neglecting any effect related to wave propagation in the viscoelastic solid since, as widely suggested in the literature (see, for example, Refs. [24,25]) we assume we are dealing with velocities much lower than the sound propagation speed.

The tangential friction force F_T needed to slide, at constant velocity $v = |\mathbf{v}|$, the viscoelastic block against the rough rigid substrate can be calculated considering that the energy per unit time W provided by the external tangential applied force F_T must balance the energy per unit time dissipated as a consequence of viscoelastic response of the material. The friction force is, therefore, easily determined as

$$W = F_T v = \int_\Omega d^2x \sigma(\mathbf{x})\mathbf{v}\cdot\nabla u(\mathbf{x}), \quad (8)$$

where Ω is the contact domain. For isotropic surfaces, we can assume, without any loss of generality, $\mathbf{v} = v\mathbf{i}$, where $\mathbf{i}$ is the unit vector of the x axis, and write the final relation as follows:

$$F_T = \int_\Omega d^2x \sigma(\mathbf{x})\frac{\partial u}{\partial x}. \quad (9)$$

The friction coefficient is then calculated as $\mu = F_T/F_N$, where F_N is the external applied load.

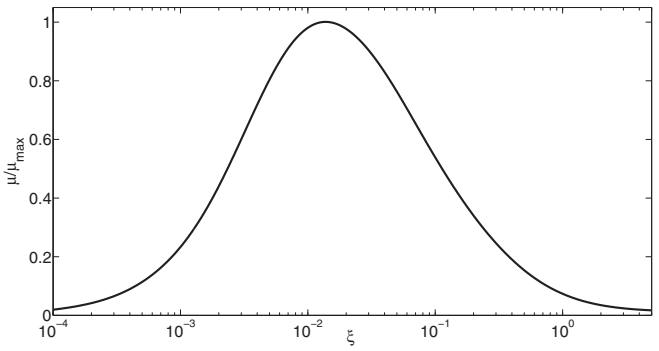

FIG. 1. The viscoelastic friction coefficient as a function of the dimensionless sliding speed ξ for a constant normal load $P = 0.30$ N.

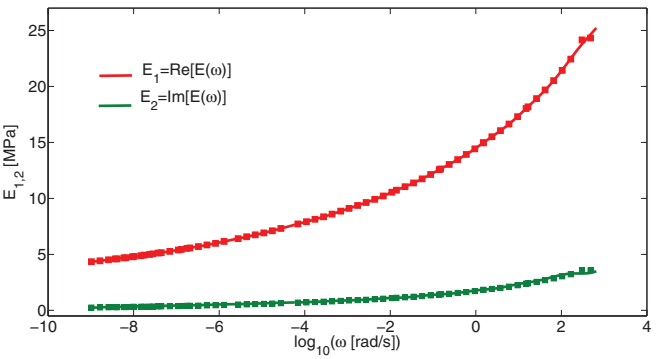

FIG. 2. (Color online) The real part $E_1 = \mathrm{Re}[E(\omega)]$ (red line) and the imaginary part $E_2 = \mathrm{Im}$ (green line) of the viscoelastic modulus $E(\omega)$ of the SBR rubber samples at a room temperature of 12 °C. Squares represent the measured values, and the solid lines denote the fit obtained according to the generalized viscoelastic models [28].

III. VISCOELASTIC FRICTION

As previously outlined, one of the parameters of major importance in viscoelastic contact mechanics is the viscoelastic friction. In this section, we show how the presented methodology can be employed to estimate the viscoelastic friction in the case of viscoelastic rough contact.

Our analysis starts from the paradigmatic case of the contact of a rigid rough fractal surface sliding over a viscoelastic half space ($h \to +\infty$) characterized by only one relaxation time. In particular, we employ for the viscoelastic material the values of $E_\infty = 10^7$ Pa, $E_\infty/E_0 = 3$, and $\tau = 0.01$ s. As for the rough surface, in this paper, we employ self-affine fractal surfaces numerically generated by means of the spectral method described in Ref. [24]. These surfaces have spectral components in the range $q_L < q < q_1$, where $q_L = 2\pi/L$, the side of the square computational cell is $L = 0.01$ m, $q_1 = Nq_L$, and N is the number of scales (or wavelengths). In particular, results shown in this section are obtained with $N = 64$.

In Fig. 1, we analyze the viscoelastic friction as a function of the dimensionless speed $\xi = (v\tau)/L$ for a fixed normal load $F_N = 0.30$ N. As expected, we have a bell-shaped curve that vanishes for very low and very high speeds, i.e., when the solid behaves as an elastic material.

Indeed, one of the main advantages of the proposed numerical methodology is the possibility to handle real viscoelastic materials characterized by a very large number of relaxation times. As a matter of fact, our approach allows us to compare numerical predictions and experimental outcomes. In our experiments, we use a rubber sample made of styrene-butadiene rubber copolymer (SBR), provided by Pirelli Tyre S.p.A. Its viscoelastic response spectrum has been characterized by dynamical mechanical analysis (DMA) carried out on the instrumentation EPLEXOR by Gabo. The real part $E_1(\omega) = \mathrm{Re}[E(\omega)]$ and the imaginary part $E_2(\omega) = \mathrm{Im}[E(\omega)]$ of the measured viscoelastic modulus $E(\omega)$ at room temperature of 12 °C are shown in Fig. 2 (see points in the figure). The solid line is the fit obtained adopting the generalized viscoelastic model with 34 relaxation times in geometric progression with Euler's number as common ratio, i.e., $\tau_{k+1}/\tau_k = e$.

As for the experimental setup (Fig. 3), we employ a very simple scheme already successfully used in Ref. [31]. Basically, the experiment consists in sliding a rubber block, with a cross section equal to $A = 1$ cm $\times$ 1 cm, and a thickness $h = 0.75$ cm, against a sandblasted randomly rough steel surface. A normal load is applied to the rubber block by means of a dead weight glued on the sample. The rubber block is pulled by a constant applied load to slide over the rough rigid substrate. Since inertia effects are negligible, the coefficient of friction can be easily calculated as the ratio between the pulling force and the normal applied force. By changing the pulling force we change the sliding velocity and therefore the friction coefficient. The sliding speed is measured as the ratio between the distance traveled by the rubber block divided by the time needed to cover the distance. The experimental procedure is here described. The rubber sample and the sandblasted plate are cleaned up by employing isopropanol. Afterwards, the normal load and the pulling force, previously weighed with a precision scale, are applied in succession. The rubber sample is allowed to slide for a certain distance and the time employed to carry out the run is measured by means of a chronometer. This procedure allows us to measure the friction coefficient as a function of the sliding speed v in a range of velocities from a few μm/s to 1 mm/s. During the experiments, the nominal contact pressure is kept constant at $p_0 = 94$ KPa, with the room temperature equal to $T = 17$ °C. We employ the time-temperature superposition principle for viscoelastic materials

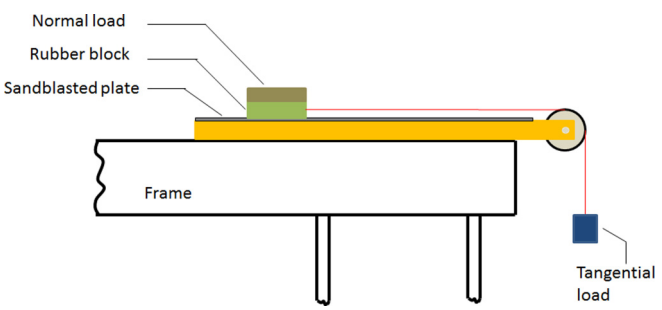

FIG. 3. (Color online) The test bench (schematic) used to measure the sliding friction of rubber. The sliding speed is controlled by pulling the sample with a weight (tangential load in the figure).

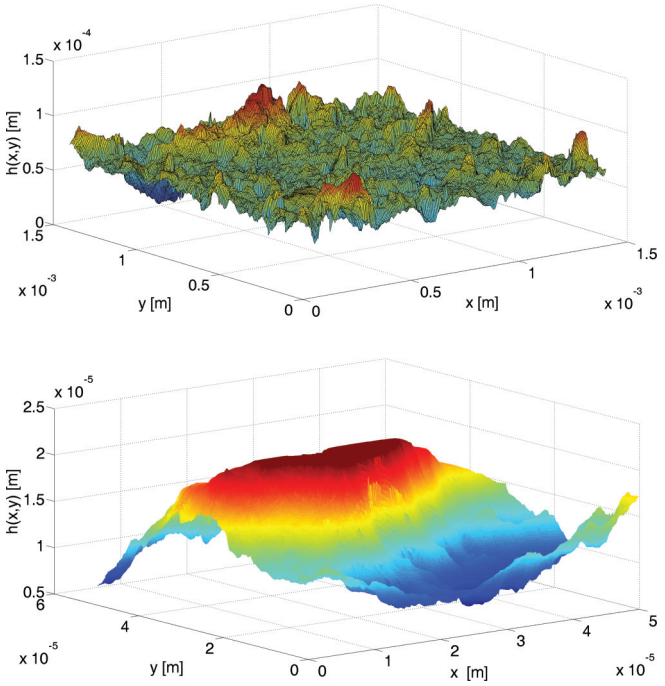

FIG. 4. (Color online) Rough contact surface obtained by use of the confocal microscope in the wave vector range $4.46 \times 10^3\ \mathrm{m}^{-1} \leqslant q \leqslant 7.94 \times 10^5\ \mathrm{m}^{-1}$ (top) and by use of the atomic force microscope in the range $1.26 \times 10^5\ \mathrm{m}^{-1} \leqslant q \leqslant 3.16 \times 10^7\ \mathrm{m}^{-1}$ (bottom).

[29] to calculate the viscoelastic spectrum of the material at 17 °C. The rough rigid substrate is made of steel, whose surface is made rough by means of sandblasting and then characterized either by the confocal microscope (CSM instruments) or the atomic force microscope (NTEGRA by NT-MDT). By use of the confocal microscope, it is possible to measure the roughness on a range of wave vectors $4.46 \times 10^3\ \mathrm{m}^{-1} \leqslant q \leqslant 7.94 \times 10^5\ \mathrm{m}^{-1}$, whereas the atomic force microscopy (AFM) measurements cover the interval $1.26 \times 10^5\ \mathrm{m}^{-1} \leqslant q \leqslant 3.16 \times 10^7\ \mathrm{m}^{-1}$. In Fig. 4, we can observe measurements obtained with the two scanning techniques.

It is worth noticing that the power spectral density (PSD) $C(\mathbf{q})$ of the rough surface shows a fractal self-affine behavior in the range $2.51 \times 10^4\ \mathrm{m}^{-1} \leqslant q \leqslant 3.16 \times 10^7\ \mathrm{m}^{-1}$ and, as clearly shown in Fig. 5, confocal microscopy measurements and atomic force microscopy measurements provide perfectly coherent measures: the AFM-measured PSD (blue color) is just the extension of the confocal microscopy-measured PSD (red color). The slope of the curve allows us to calculate the fractal dimension of the surface which is close to $D_f = 2.18$, corresponding to a Hurst coefficient $H = 0.82$. In order to carry out a comparison between predictions and experiments, we have numerically generated different realizations of a surface with $H = 0.82$ and wave-vector values covering the interval $2.51 \times 10^4\ \mathrm{m}^{-1} \leqslant q \leqslant 6.31 \times 10^6\ \mathrm{m}^{-1}$ (corresponding to wavelengths in the range from 1 μm to 2.6 mm). The resulting PSD is shown in Fig. 5 in yellow; the overlapping with the measured one is perfect. Observe that the short-length cut-off vector q_1 of the numerically generated surface is smaller than the one obtained with AFM measurements. This is because

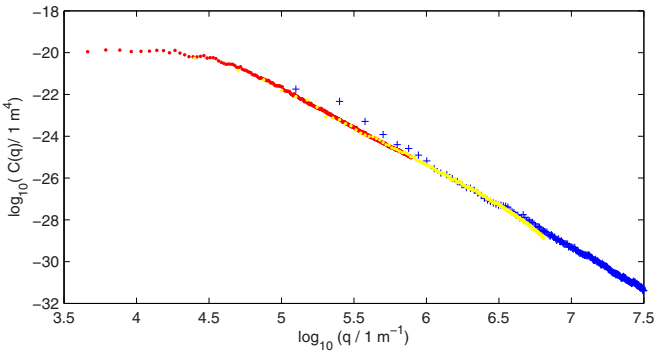

FIG. 5. (Color online) Power spectral density $C(\mathbf{q})$ of the rough surface. Red dots refer to confocal measures, blue crosses to AFM measures, and yellow dots to the numerically generated surface employed for the theoretical predictions.

we expect that dust particles of size of order ~ 1 μm filter out the shorter-wavelength component of the roughness PSD. However, we note that determining the cut-off vector q_1 needed to carry out friction calculations, i.e., determining how many scales N contribute to the viscoelastic friction, is an open question in modern tribology (see, for example, Ref. [4]). The viscoelastic friction is, indeed, significantly dependent on the short-length cut-off wave vector $q_1 = 2\pi N/L_0$ and, in particular, monotonically increases with q_1 [4]. As a consequence, in theoretical predictions, q_1 appears as a free parameter. To close the problem, a criterion should be proposed to determine the proper value of q_1. As an example, in the case of a tire sliding on a asphalt road, the quantity q_1 may be related to the micrometer size of the small dirt particles covering the contacting surfaces or, alternatively, can be related to the size of rubber wear particles. However, the definition of the proper criterion is beyond the purpose of the present study. In order to compare numerical predictions and experiments, we need to observe that, during the tests, the measured friction coefficient μ is the sum of two contributions: one term is almost constant and equal to the interfacial Coulomb friction μ_C (and therefore independent on the sliding speed), the second contribution

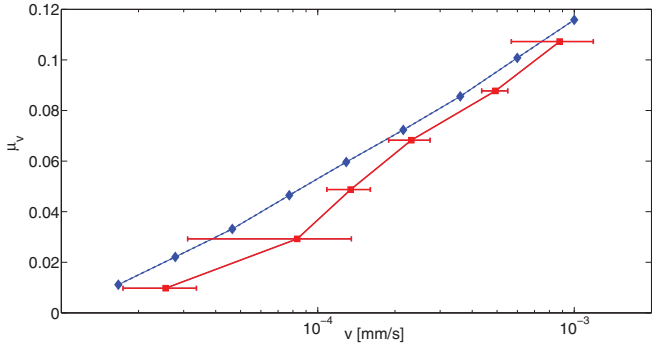

FIG. 6. (Color online) The viscoelastic friction μ_V for different sliding speeds v, given a normal constant pressure $p_0 = 94$ KPa. The numerical calculated values (blue rhomboids) are compared to the measured ones (red squares). Red lines are referred to the standard deviation of the experimental outcomes. Notice that the x axis is in a logarithmic scale.

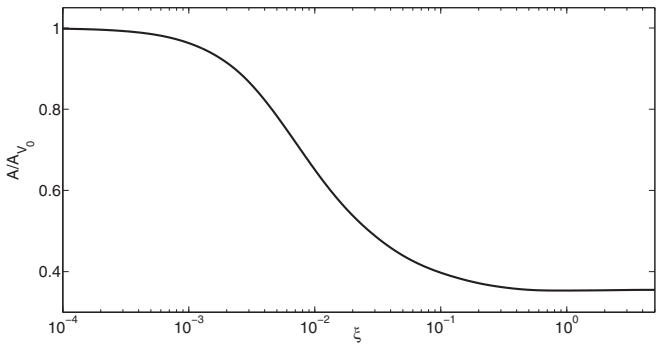

FIG. 7. Dimensionless contact area A/A_{v_0} as a function of the dimensionless sliding speed ξ for a constant normal load $P = 0.30$ N.

is instead related to viscoelastic energy dissipation in the bulk of the material and clearly influenced by the sliding speed. In order to extract the contribution of the viscoelastic friction we simply subtract the constant term μ_C, measured at extremely small sliding velocity, from the total coefficient of friction μ; therefore the quantity $\mu_V = \mu - \mu_C$ should be representative of the viscoelastic friction contribution. In Fig. 6, the term μ_V is plotted as a function of the sliding speed v. The agreement between experimental outcomes and numerical results is relatively good and supports the proposed methodology. Incidentally, we observe that, since the thickness of the viscoelastic slab, is much greater than the roughness wavelengths ($h \gg 2\pi/q_L$ being q_L the roll-off wave vector equal to $q_L = 4.46 \times 10^3$ m^{-1}), no corrective factor has been necessary to account for the finite thickness of the rubber sample.

IV. CONTACT ANISOTROPY INDUCED BY VISCOELASTICITY

Once the numerical model has been validated, it is possible to focus on the second effect marking the strong peculiarity of viscoelastic sliding contact: This is the contact anisotropy. In order to enlighten paradigmatically such a phenomenon, we employ the one-relaxation-time material defined in the previous section.

Our analysis starts from a quantitative analysis of the real contact area A. In Fig. 7, for a nominal contact pressure $\sigma_0 = F_N/L^2 = 3$ kPa, we study, as a function of the dimensionless quantity $\xi = v\tau_0/L$, the ratio A/A_{v_0} between the real contact

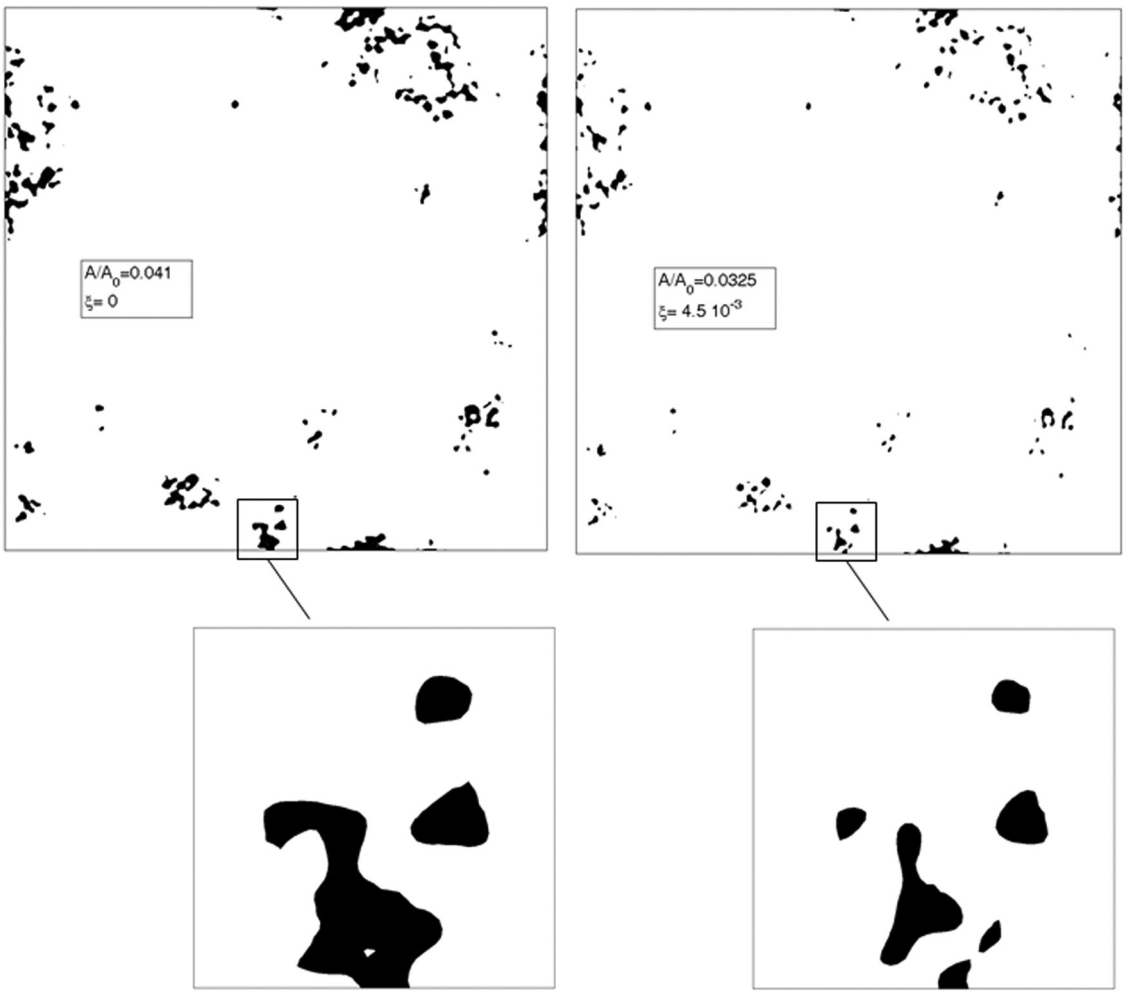

FIG. 8. Real contact area for $\xi = 0$ (left) and $\xi = 4.5 \times 10^{-3}$ (right), given a constant normal load $P = 0.30$ N. The same region is extracted to enlighten anisotropic effects.

area A and the real contact area in stationary conditions $A_{v_0} = A(\xi = 0)$, when the material is completely relaxed. As expected, due to the viscoelastic stiffening, the contact area decreases as the dimensionless sliding velocity ξ is increased. Interestingly, if we focus our attention on the ratio $A(\xi)/A_{v_0}$, we expect that this quantity must approach the value $E_0/E_\infty = 1/3$ at large sliding velocity, since in this case the behavior of the material is elastic. This is clearly shown in Fig. 7 and is a consequence of the direct proportionality of the intimate contact area on the ratio between the nominal applied pressure and the composite elastic modulus (for elastic contacts, see Refs. [4,16,25]), i.e.,

$$\frac{A}{A_0} = \frac{\kappa}{\sqrt{\langle \nabla h \rangle^2}} \frac{\sigma_0}{E^*}, \tag{10}$$

where A_0 is the nominal contact area, E^* is the composite Young's modulus $E^* = E/(1-\nu^2)$, and κ is a constant proportionality coefficient proved to be very close to 2 [25].

Figure 8 shows that, in addition to the decrease of contact area, increasing ξ leads a marked shrinkage of the contact area at the trailing edge. This is particularly evident in the magnified views of Fig. 8. Therefore, despite the isotropy of the rigid randomly rough surface, the interfacial displacement field of the viscoelastic solid (i.e., the shape of the deformed surfaces) will show a certain degree of anisotropy.

To quantify the degree of anisotropy of the deformed surface in a certain range of wave vectors $\zeta_1 q_0 < |\mathbf{q}| < \zeta_2 q_0$, one can use the (symmetric) anisotropy tensor defined as

$$\mathbf{M}(\zeta_1,\zeta_2) = \int_{\zeta_1 q_0 < |\mathbf{q}| < \zeta_2 q_0} d^2q\, \mathbf{q} \otimes \mathbf{q} C(\mathbf{q}), \tag{11}$$

where $C(\mathbf{q}) = (2\pi)^{-2} \int d^2x \langle u(\mathbf{0};\zeta_1,\zeta_2) u(\mathbf{x};\zeta_1,\zeta_2)\rangle \exp(-i\mathbf{q}\cdot\mathbf{x})$ is the power spectral density of the filtered deformed surface $u(\mathbf{x};\zeta_1,\zeta_2)$ (the symbol $\langle\rangle$ stands for the ensemble average). Observe that the quantity $M_{ij} = \int_{\zeta_1 q_0 < |\mathbf{q}| < \zeta_2 q_0} d^2q q_i q_j C(q)$, with i and $j = 1,2$, corresponds to the second-order moments of the power spectral density of the filtered surface, i.e., $M_{11} = m_{20} = \langle u_x^2 \rangle$, $M_{22} = m_{20} = \langle u_y^2 \rangle$, and $M_{12} = m_{11} = \langle u_x u_y \rangle$, where $u_x = \partial u/\partial x$, $u_y = \partial u/\partial y$ (see also Ref. [32]). Incidentally, we observe that if the range $[\zeta_1,\zeta_2]$ is too wide, in order to balance the dominant contribution of large wave vectors, it would be preferable to define the anisotropic tensor as [33]

$$\mathbf{M}(\zeta_1,\zeta_2) = \int_{\zeta_1 q_0 < |\mathbf{q}| < \zeta_2 q_0} d^2q \frac{\mathbf{q}\otimes\mathbf{q}}{|\mathbf{q}|^2} C(\mathbf{q}). \tag{12}$$

However, in our case, the two definitions do not lead to significantly qualitative differences and we will use formulation (11). Furthermore, associated to the symmetric tensor $\mathbf{M}$, one can conveniently use the quadratic form $Q(\mathbf{x}) = M_{ij} x_i x_j$. Letting $x = r\cos\theta$ and $y = r\sin\theta$, one easily obtains the following:

$$Q(\mathbf{x}) = r^2 |\nabla h \cdot \mathbf{e}(\theta)|^2 = r^2 m_2(\theta),$$

where $\mathbf{e}(\theta)$ is the unit vector $(\cos\theta, \sin\theta)$ and

$$m_2(\theta) = m_{20}\cos^2(\theta) + 2m_{11}\sin(\theta)\cos(\theta) + m_{02}\sin^2(\theta) \tag{13}$$

is simply the average square slope of the a profile obtained by cutting the deformed surface $u(\mathbf{x};\zeta_1,\zeta_2)$ along the direction θ [34]. The quantity $m_2(\theta)$ can be represented in a polar diagram: A circumference means isotropy, otherwise the surface is anisotropic.

To characterize the anisotropy of the deformed surface, one can define the degree of isotropy as the ratio $\gamma = m_{2\min}/m_{2\max}$ between the minimum $m_{2\min}$ and the maximum $m_{2\max}$ eigenvalues of the tensor $\mathbf{M}$, and the principal directions of anisotropy through the eigenvectors of the tensor $\mathbf{M}$, e.g., by the value of the angle θ_P which maximizes $m_2(\theta)$, i.e., $m_2(\theta_P) = m_{2\max}$. In this analysis, we use $\zeta_1 = 1$ and $\zeta_2 = N = 64$ to obtain the polar diagram shown in Fig. 9. We notice that, unlike what happens at zero sliding speed, where the deformed surface is almost perfectly isotropic (a circular polar diagram is shown in Fig. 9 with $\gamma = 0.93$, very close to 1), at nonzero sliding velocity, e.g., for ξ equal to 1.17×10^{-2},

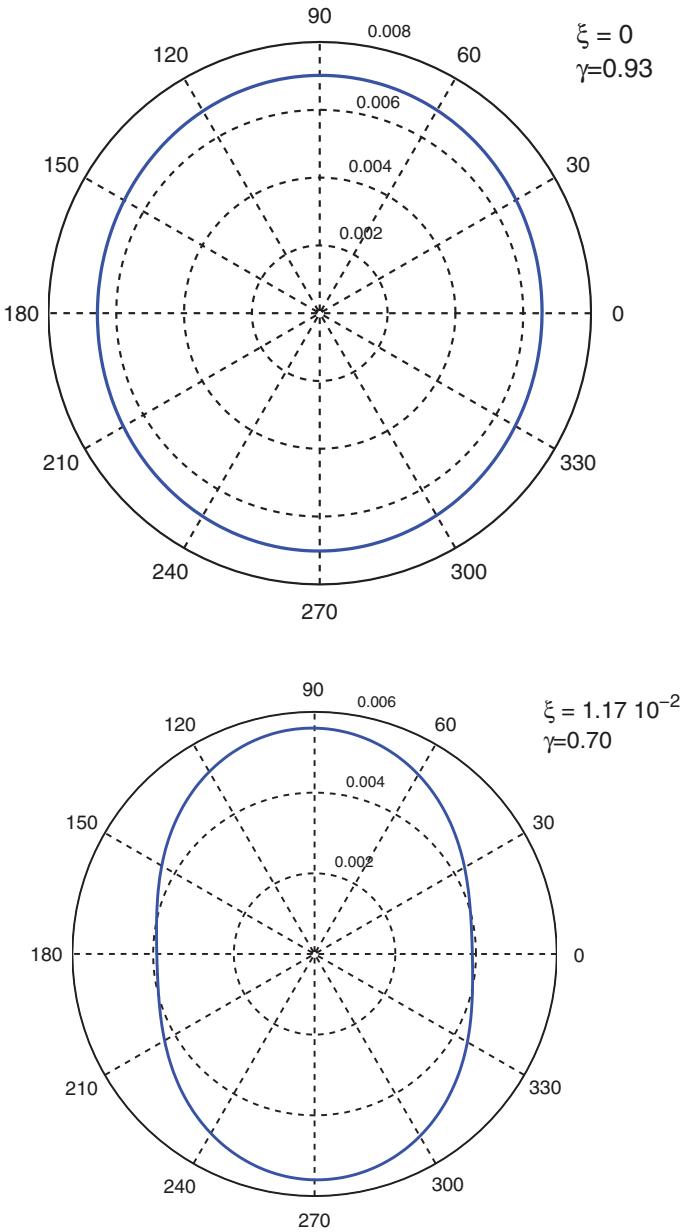

FIG. 9. (Color online) Polar plots of $m_2(\theta)$ for $\xi = 0$ and $\xi = 1.17 \times 10^{-2}$ given a constant normal load $P = 0.30$ N.

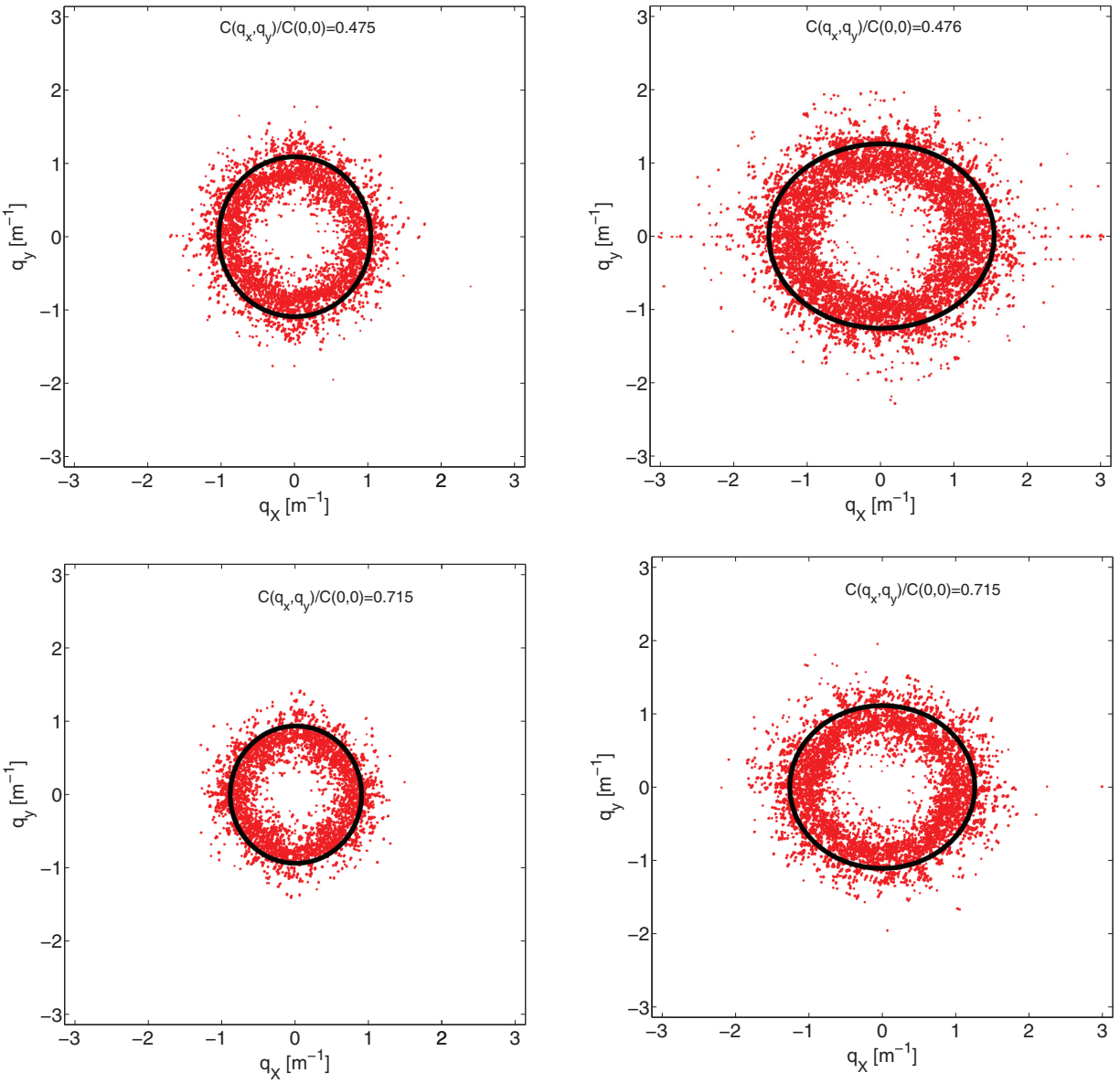

FIG. 10. (Color online) Contours of $C(\mathbf{q})$ for stationaty conditions (left) and for a dimensionless speed $\xi = 1.17 \times 10^{-2}$ (right). Red dots refers to punctual values of $C(\mathbf{q})$; black lines are elliptical fits.

which correspond to the maximum degree of anisotropy, $\gamma = 0.70$. Interestingly, the speed $\xi = 1.17 \times 10^{-2}$, for which we find the greatest anisotropy, is the value where the maximum viscoelastic friction is found. This confirms that anisotropy and friction are strictly connected and both related to the loss modulus Im$[(E(\omega)]$, i.e., to the parameter governing the viscoelastic friction. Furthermore, the principal direction θ_P is almost perfectly parallel to the sliding speed (i.e., to the x axis). This is fully consistent with results shown in Fig. 8, where the contact area looks stretched along the y axis.

We notice that the methodology just employed to quantify the anisotropy is based on the analysis of the deformed surface and, although it has the important advantage of dealing with quantities familiar to the scientific community, like m_2, it could become less effective when considering very small contact areas. Indeed, in this last case, since the analysis is carried out on the total computational domain, the very large noncontact regions tend to blur the anisotropic contributions. An alternative way to quantify the anisotropy can rely directly on the contact area. Indeed, given the contact area, we can define the characteristic function $\chi(\mathbf{x})$ equal to 1 if $\mathbf{x}$ belongs to the contact region or, otherwise, to 0. Now, if we calculate the power spectral density $C_\chi(\mathbf{q})$ of $\chi(\mathbf{x})$, in the case of an anisotropic contact area, $C_\chi(\mathbf{q})$ will be itself anisotropic. Indeed, in Fig. 10, for two fixed values of the dimensionless ratio $C_\chi(\mathbf{q})/C_\chi(\mathbf{0})$, we observe on the left the contours in stationary conditions and on the right those for the speed corresponding to the greatest anisotropy. In the first case, the contours lines are circumferences, whereas in the latter we have ellipselike shapes stretched in the speed direction. This is perfectly coherent with the contact area shrinkage in the direction of speed, since the spatial frequency are clearly related to the inverse of the spatial vectors. In this case, the degree of anisotropy can be quantified by the ratio λ between

the smallest and the greatest ellipses axis. In the specific case here considered, we find $\lambda \simeq 0.8$, which is quite close to the value of γ in the same conditions.

V. CONCLUSION

In this paper, we employ the numerical theory developed by the authors in Ref. [13] to study the sliding contact mechanics between a viscoelastic solid and a rigid randomly rough surface. Numerical calculations show that, in comparison with the elastic contact problem, viscoelasticity has a very strong influence on the solution. We carry out numerical calculations to estimate the viscoelastic friction as a function of the sliding speed. The theoretical predictions are then compared to experimental observation. A good agreement between numerical simulations and the measured friction coefficient supports the validity of the proposed numerical approach.

Finally, we focus on the contact area and on its anisotropy. Indeed, given the applied load, one observes a significant reduction of the contact area due to the viscoelastic stiffening which occurs as the sliding velocity increases. The real contact area shrinking is associated to a marked increase of anisotropy of the contact areas, which are stretched along the direction perpendicular to the sliding speed. Two different methodologies are proposed to quantify the degree of anisotropy; the first relies on the analysis of the slope distribution of the viscoelastic deformed surface, and the second, instead, analyses the power spectral density of characteristic function of the contact area.

ACKNOWLEDGMENTS

The authors thank the support of the Italian Ministry of Education, University and Research, within the Projects PON01 02238 and PON02 00576 3333604. C.P. also gratefully acknowledges the support of Marie Curie IEF fellowship SOFT-MECH (Grant No. 622632).

APPENDIX: SOME COMMENTS ON FFT APPROACH TO VISCOELASTIC CONTACT PROBLEMS

By relying on the viscoelastic correspondence principle, Eq. (1) can be simply rewritten in the Fourier space as follows:

$$\sigma\left(\mathbf{q},\omega\right) = M^{-1}\left(\mathbf{q},\omega\right) u\left(\mathbf{q},\omega\right), \tag{A1}$$

with $M(\mathbf{q},\omega)$ being the correction response function (see Ref. [14] for more details). Now considering that in our case the sliding velocity $\mathbf{v}$ is constant and the system is in steady-state conditions, one has where $\sigma(\mathbf{q},\omega) = \sigma(\mathbf{q})\delta(\omega - \mathbf{q}\cdot\mathbf{v})$, $u(\mathbf{q},\omega) = u(\mathbf{q})\delta(\omega - \mathbf{q}\cdot\mathbf{v})$, which, together with Eq. (A1), gives

$$\sigma\left(\mathbf{q}\right) = M^{-1}\left(\mathbf{q},\mathbf{q}\cdot\mathbf{v}\right) u\left(\mathbf{q}\right). \tag{A2}$$

In principle, employing Eq. (A1) together with fast Fourier transform (FFT) methods could be a powerful tool to solve viscoelastic contact problems, since Eq. (A1), unlike Eq. (1), does not require solving a linear system but simply to carry out a multiplication. Moreover, the viscoelastic friction force can be easily determined considering that viscoelastic energy loss per unit time, $P = F_T v = \int d^2x\, \dot{u}\sigma$, can be rephrased in Fourier space as

$$P = (2\pi)^2 \int d^2q\, (i\mathbf{q}\cdot\mathbf{v})\, M^{-1}\left(\mathbf{q},\mathbf{q}\cdot\mathbf{v}\right) |u\left(\mathbf{q}\right)|^2, \tag{A3}$$

from which we obtain the following:

$$F_T = (2\pi)^2 \int d^2q (i\mathbf{q}\cdot\mathbf{e}_v) M^{-1}\left(\mathbf{q},\mathbf{q}\cdot\mathbf{v}\right) |u\left(\mathbf{q}\right)|^2, \tag{A4}$$

where $\mathbf{e}_v = \mathbf{v}/v$. However, we observe that, in addition to these computational advantages, there are also possible drawbacks when dealing with a nonperiodic domain. Indeed, the solution scheme in the Fourier space needs to solve the problem not only in the contact areas (as we do in the case of the real space formulation proposed in the previous sections) but in all the nominal computational domain. The crucial question is, therefore, how to choose the computational cell since it will influence the contact solution. The best choice would be to have a computational domain that extends far beyond the relaxation length $l = v\tau$, where τ is the relaxation time of the material. However, real viscoelastic materials possess relaxation times spanning more than 8–10 orders of magnitude, thus making the length l of the computation domain hugely large. This of course requires the use of an extremely large number of grid points and has to be taken in proper consideration when FFT-based approaches are employed to analyze these types of contacts.

[1] S. C. Hunter, J. Appl. Mech. **28**, 611 (1961).
[2] B. N. J. Persson, Eur. Phys. J. E **33**, 327 (2010).
[3] C. Panek and J. J. Kalker, IMA J. Appl. Math. **26**, 299 (1980).
[4] B. N. J. Persson, J. Chem. Phys. **115**, 3840 (2001).
[5] B. N. J. Persson, J. Phys.: Condens. Matter **18**, 7789 (2006).
[6] P. Le Tallec and C. Rahler, Int. J. Numer. Methods Eng. **37**, 1159 (1994).
[7] E. A. H. Vollebregt, VORtech Computing Technical Report No. TR09-03, version 13.1, 2013.
[8] J. Padovan and O. Paramadilok, Comput. Struct. **20**, 545 (1985).
[9] J. Padovan, Comput. Struct. **27**, 249 (1987).
[10] J. Padovan, A. Kazempour, F. Tabaddor, and B. Brockman, Finite Elem. Anal. Des. **11**, 275 (1992).
[11] U. Nackenhorst, Comput. Methods Appl. Mech. Eng. **193**, 4299 (2004).
[12] L. Nasdala, M. Kaliske, A. Becker, and H. Rothert, Computat. Mech. **22**, 395 (1998).
[13] G. Carbone and C. Putignano, J. Mech. Phys. Solids **61**, 1822 (2013).

[14] G. Carbone and L. Mangialardi, J. Mech. Phys. Solids **52**, 1267 (2004).
[15] C. Putignano, T. Reddyhoff, G. Carbone, and D. Dini, Tribol. Lett. **51**, 105 (2013).
[16] J. A. Greenwood and J. B. P. Williamson, Proc. R. Soc. London A **295**, 300 (1966).
[17] J. A. Greenwood, C. Putignano, and M. Ciavarella, Wear **270**, 332 (2011).
[18] A. W. Bush, R. D. Gibson, and T. R. Thomas, Wear **35**, 87 (1975).
[19] G. Carbone and F. Bottiglione, J. Mech. Phys. Solids **56**, 2555 (2008).
[20] G. Carbone, M. Scaraggi, and U. Tartaglino, Eur. Phys. J. E **30**, 65 (2009).
[21] G. Carbone and E. Pierro, J. Adhes. Sci. Technol. **26**, 2555 (2012).
[22] C. Campana, B. N. J. Persson, and M. H. Mueser, J. Phys.: Condens. Matter **23**, 085001 (2011).
[23] C. Campana, M. H. Mueser, and M. O. Robbins, J. Phys.: Condens. Matter **20**, 354013 (2008).
[24] C. Putignano, L. Afferrante, G. Carbone, and G. Demelio, Int. J. Solids Struct. **49**, 338 (2012).
[25] C. Putignano, L. Afferrante, G. Carbone, and G. Demelio, J. Mech. Phys. Solids **60**, 973 (2012).
[26] C. Putignano, L. Afferrante, G. Carbone, and G. P. Demelio, Tribol. Int. **64**, 148 (2013).
[27] M. Scaraggi, C. Putignano, and G. Carbone, Wear **297**, 811 (2013).
[28] R. M. Christensen, *Theory of Viscoelasticity*, 1st ed. (Academic Press, New York, 1982).
[29] M. L. Williams, R. F. Landel, and J. D. Ferry, J. Am. Chem. Soc. **77**, 3701 (1955).
[30] K. L. J. Johnson, *Contact Mechanics* (Cambridge University Press, Cambridge, 1985).
[31] G. Carbone, B. Lorenz, B. N. J. Persson, and A. Wohlers, Eur. Phys. J. E **29**, 275 (2009).
[32] M. S. Longuet-Higgins, Phil. Trans. R. Soc. London A **249**, 321 (1957).
[33] M. Scaraggi, G. Carbone, B. N. J. Persson, and D. Dini, Soft Matter **7**, 10395 (2011).
[34] J. I. McCool, Wear **49**, 19 (1978).